ARTICLE

# High-Efficiency Solid-State Dye-Sensitized Solar Cells: Fast Charge Extraction through Self-Assembled 3D Fibrous Network of Crystalline $TiO_2$ Nanowires

**Nicolas Tétreault,[†,*] Endre Horváth,[‡] Thomas Moehl,[†] Jérémie Brillet,[†] Rita Smajda,[‡] Stéphane Bungener,[‡] Ning Cai,[⊥] Peng Wang,[⊥] Shaik M. Zakeeruddin,[†] László Forró,[‡] Arnaud Magrez,[‡,§,*] and Michael Grätzel[†]**

[†]Laboratory of Photonic and Interfaces, Institute of Physical Chemistry, [‡]Laboratory of Physics of Complex Matter, Institute of Condensed Matter Physics, and [§]Center for Research on Electronically Advanced Materials, Institute of Condensed Matter Physics, École Polytechnique Fédérale de Lausanne, 1015 Lausanne, Switzerland and [⊥]State Key Laboratory of Polymer Physics and Chemistry, Changchun Institute of Applied Chemistry, Chinese Academy of Sciences, Changchun 130022, China

**ABSTRACT** Herein, we present a novel morphology for solid-state dye-sensitized solar cells based on the simple and straightforward self-assembly of nanorods into a 3D fibrous network of fused single-crystalline anatase nanowires. This architecture offers a high roughness factor, significant light scattering, and up to several orders of magnitude faster electron transport to reach a near-record-breaking conversion efficiency of 4.9%.

**KEYWORDS:** hybrid materials · photovoltaic devices · solar cells · titanium dioxide · nanowires

Dye-sensitized solar cells (DSCs) are one of the most promising photovoltaic technologies for production of renewable, clean, and affordable energy. Liquid electrolyte-based DSCs have reached efficiencies as high as 11.1%.[1−3] However, these liquid-based DSCs may suffer from potential leakage and corrosion problems;[4,5] the potential disadvantages have sparked research in DSCs that have solid-state hole transport materials (HTMs) instead of liquid electrolytes. One of the most widely used HTMs is spiro-MeOTAD (2,2′,7,7′-tetrakis-(*N*,*N*-di-*p*-methoxyphenylamine)9,9′-spirobifluorene).[6] Devices with spiro-MeOTAD as HTM have already attained efficiencies over 5%,[7,8] which is still below the efficiency of liquid electrolyte DSCs. The lower efficiency is primarily a consequence of incomplete light harvesting. Indeed, high-performance solid-state DSCs (ss-DSCs) are still limited to a 2−3 μm thick active layer that is far thinner than needed to achieve good optical absorption for most of the currently used sensitizers.[9] There are two factors that limit the ss-DSCs from being more efficient at a thickness of >2 μm: incomplete filling of the mesoporous $TiO_2$ films with spiro-MeOTAD and electron−hole recombination. Studies show that recombination is 2 orders of magnitude faster and electron diffusion length is 1 order of magnitude lower in ss-DSCs than in liquid DSCs.[10−13] Pore filling has been the focus of a thorough study that linked the cell efficiency and optimal thickness to the pore filling by way of varying the spinning speed and concentration of spiro-MeOTAD in the infiltrating solution.[14] However, the optimal thickness remained below 3 μm.

Electron transport in DSCs is governed by an ambipolar diffusion mechanism controlled by trap-limited hopping through a relatively long and tortuous path to the transparent substrate.[15−17] Given a charge collection time of milliseconds at the maximum power point,[18] efficient charge extraction is only made possible through the extraordinarily slow interception of electrons by adjacent $I_3^-$. However, this recombination pathway is 2 orders of magnitude faster in ss-DSCs, which makes it one of the main limiting factors in their efficiency. Several approaches have been proposed in order to improve charge collection in liquid electrolyte and ss-DSCs including the use of radial collection nanostructures[19] and one-dimensional ZnO and $TiO_2$ nanorods and nanowires as photoanodes.[20−23] Even though these approaches show great promise, they have yet to achieve power conver-

*Address correspondence to nicolas.tetreault@epfl.ch, arnaud.magrez@epfl.ch.

Received for review September 17, 2010 and accepted November 04, 2010.

**Published online November 17, 2010.** 10.1021/nn1024434

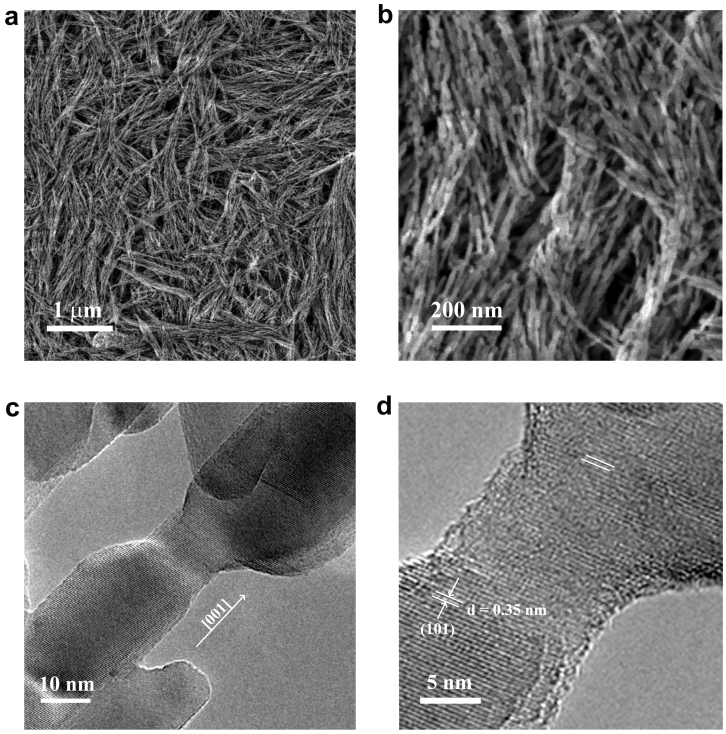


**Figure 1. Oriented attachment of nanorods into a 3D fibrous network of single-crystalline anatase nanowires. (a) High-resolution scanning electron micrograph of the top surface showing nanowire aggregates and the macroporous structure. (b) Oriented self-assembly of the nanorods into the 3D fibrous network. (c) High-resolution transmission electron micrograph showing the continuous [001] crystal orientation across two nanorods. (d) Continuous (101) crystal plane and spacing across the junction.**

sion efficiencies above 5% in liquid electrolyte DSCs and 1.7% in ss-DSCs.

One of the major issues with these novel photoanodes is their limited roughness factor which greatly limits dye loading and, ultimately, absorption and photocurrent. In liquid DSCs, improved light harvesting has been demonstrated using backscattering overlayer,[24] mesoporous macroparticles,[25] mixtures of macroparticles and nanoparticles,[1] as well as photonic crystals.[26−28] However, the limited thickness in ss-DSCs prohibits the use of these different strategies and necessitates the development of thin-film electrodes that are inherently diffusive.

## RESULTS AND DISCUSSION

Herein, we present the first high-efficiency ss-DSC built using a three-dimensional (3D) fibrous network of anatase nanowires self-assembled from fused single-crystal nanorods. This novel photoanode material is the first to incorporate a high-conductivity network for efficient electron extraction, a relatively high roughness factor for dye loading, and large pores for enhanced light harvesting through light scattering. From high-resolution scanning and transmission electron microscopy (HRSEM and TEM), it is found that the 3D fibrous network is formed of primary $TiO_2$ nanorods that self-assemble into interconnected single-crystalline nanowires. This morphology offers large pores that efficiently scatter light to enhance light harvesting and a high roughness factor of 144 that permits adequate dye loading. A detailed study using electrochemical impedance spectroscopy (EIS) shows that this 3D morphology presents a significantly higher conductivity over a wide range of applied potential as well as faster electron transport than comparable nanoparticle-based ss-DSCs which result in improved collection efficiencies. Using a state-of-the-art organic dye,[29] these factors combine to achieve the highest reported power conversion efficiency in a nanowire-based solid-state device of 4.9% under AM1.5. This result puts this novel morphology in direct competition with conventional nanoparticle-based ss-DSCs, which until recently were capable of achieving only slightly higher power conversions than 5% (AM1.5).[7,8]

The primary building block of this 3D fibrous network is the single-crystal nanorod. These subparticles are obtained from the thermal decomposition of titanate nanowires between 20 and 60 nm in diameter and 1 and 20 μm in length (see Supporting Information, Figures S1 and S2). Nanowires are produced by a two-step hydrothermal process. In a typical synthesis, a mixture of anatase and NaOH solution is treated at 130 °C for 36 h. The resulting white powder undergoes a second hydrothermal treatment at 200 °C while mixed with KOH. The obtained nanowires are subsequently collected, washed, and dried at 250 °C. In order to produce a solution for doctor blading that would both exhibit good wettability on FTO glass substrate and produce smooth thin films, the nanowires are sonicated in isopropyl alcohol for 30 min. The nanowire solution of 24 mg/mL in isopropyl alcohol is then doctor bladed using a 40 μm spacer (3M) to obtain the desired film thickness of 2.5 μm.

The nanowires go through an oriented attachment growth mechanism to form a 3D network of nanorods.[30] At first, nanowires self-assemble in two dimensions parallel to the FTO glass substrate during the doctor blading process. The network consequently condenses during the evaporation of isopropyl alcohol, enhancing the number of contact points between the individual nanowires (Figure 1a). During the subsequent thermal decomposition, each titanate nanowire undergoes a transformation into chain-like assembly of truncated anatase nanorods (Figure 1b,c).[31] Figure 1c,d shows high-resolution

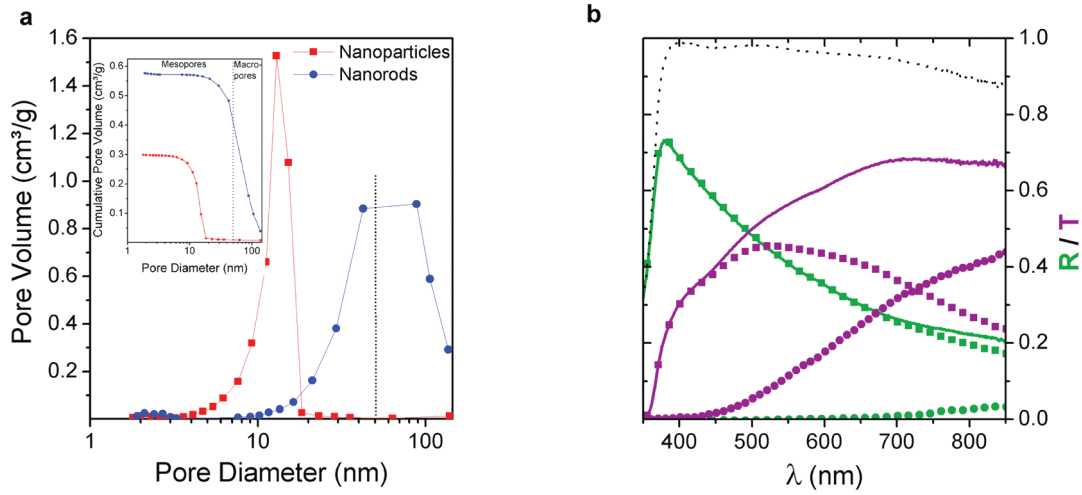


**Figure 2. Physical and optical properties of the 3D fibrous network electrode. (a) Comparison of the pore volume and diameter for thin-film electrode made of conventional 23 nm anatase nanoparticles (red) and the 3D fibrous network of anatase nanowires (blue). (b) Total transmittance (purple, solid) and reflectance (green, solid) in a 2.5 μm thick 3D fibrous network thin film on FTO glass substrate including the specular (round dots) and diffused (square dots) contributions. Black dotted line represents the total amount of light measured.**

TEM images of the interconnected $TiO_2$ nanorods elongated in the [001] direction. All images clearly show single-crystalline nanorods with lattice fringes of the (101) plane obtained. The analysis of the interface between two attached nanorods reveals reduced lattice fringes' misorientation through grain boundaries from one particle to the next, confirming the topotactic transformation of the nanowires.[32] Oriented attachment also occurs spontaneoulsy at the contact point between nanowires to yield a stabilized 3D network of nanorods with enhanced grain boundaries.[30] The crystal structure of the 3D network of nanorods is confirmed by the XRD peak positions obtained which are consistent with the standard powder diffraction pattern of the pure anatase phase of $TiO_2$ (JCPDF 21-1272) with no secondary phase or rutile formation observed. An averaged primary crystallite size of 13.6 nm is predicted from the full width at half-maximum value of the (101) XRD peak using Scherrer's equation. This is in good agreement with the average nanorod diameter obtained by analyzing TEM images (12 ± 3 nm; see Supporting Information, Figures S1 and S2).

Using a nitrogen adsorption−desorption technique, the specific surface area, pore diameter, and pore volume for the fibrous anatase network are compared with that of conventional films obtained from a 23 nm anatase nanoparticles paste prepared in-house (Figure 2a).[33] Conventional films offer a narrow pore size distribution in the mesoporous regime ranging from 4 to 18 nm, while the average pore size is centered at 13 nm and the corresponding total pore volume is about 0.3 $cm^3/g$. By comparison, the 3D network of nanorods exhibits a wide pore size distribution composed of large 10−50 nm mesopores and 50−120 nm macropores. The films' porosity is about 40% higher than that of conventional films resulting in almost double the total volume of pores (0.58 $cm^3/g$) with the majority (75%) of these pores being larger than 50 nm. This is the result of low packing density of the nanowires due to their large anisotropy (see Supporting Information, Figure S3) and allows for efficient infiltration with the HTMs. In fact, the observed hysteresis in the pressure isotherm shows a H3 feature generally associated with aggregates of thin, flaky particles giving rise to slit-shaped pores. Finally, nanorod and nanoparticle-based films exhibit a BET surface area of 60 and 83 $m^2/g$, respectively. Although the 144 roughness factor of the 3D architecture of nanorods developed in this study is higher than in previous nanowire-based ss-DSCs, it remains lower than the 374 roughness factor of conventional films. Consequently, the dye loading is reduced and would greatly limit light harvesting if it occurred in transparent, nanoparticle-based films (see Supporting Information, Figure S4 and Table S1).

However, lower dye loading in the 3D network film is partly compensated by significant light scattering in the film. Indeed, Chiba *et al.* have shown that efficient light scattering significantly increases light harvesting in the DSC and, consequently, its photocurrent.[1] In the nanowire-based photoanode, the aggregation mechanism provides for both large aggregates and macropores (Figure 1a) capable of effective light scattering, as can be seen in Figure 2b. About 20−40% of visible light is scattered in transmission and reflection for 2.5 μm thick films.

Complete DSC devices were prepared using 2.5 μm doctor bladed thin films on FTO glass. After calcination in air at 600 °C for 2 h, the thin film is dipped overnight in an acetonitrile solution of C218 high extinction coefficient organic dye.[29] The thin film is then ready to be infiltrated with a solution of spiro-MeOTAD hole trans-

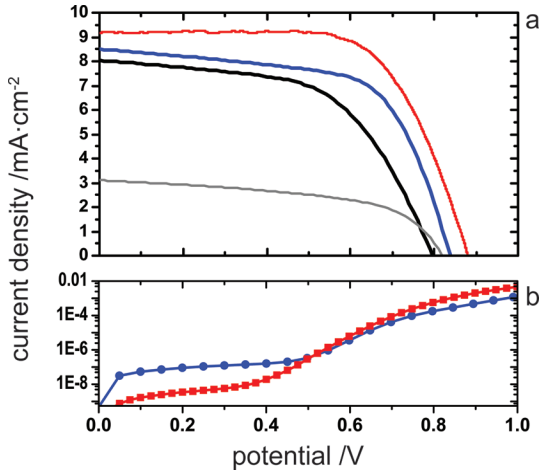


**Figure 3. Photocurrent density−voltage ($J-V$) characteristics of the 3D fibrous network and nanoparticle-based ss-DSCs. (a) $J-V$ characteristics for the as-prepared (gray, $J_{sc}$ = 3.1 mA/cm$^2$, $V_{oc}$ = 820 mV, FF = 0.55, $n$ = 1.5%), $TiCl_4$-treated (black, $J_{sc}$ = 8.0 mA/cm$^2$, $V_{oc}$ = 795 mV, FF = 0.56, $n$ = 3.9%), ALD-treated electrodes (blue, $J_{sc}$ = 8.50 mA/cm$^2$, $V_{oc}$ = 838 mV, FF = 0.63, $n$ = 4.9%), and $TiCl_4$-treated nanoparticle-based cell (red, $J_{sc}$ = 9.1 mA/cm$^2$, $V_{oc}$ = 881 mV, FF = 0.67, $n$ = 5.4%). (b) Comparison of the dark current for a conventional nanoparticle film (red) and the 3D fibrous network film (blue).**

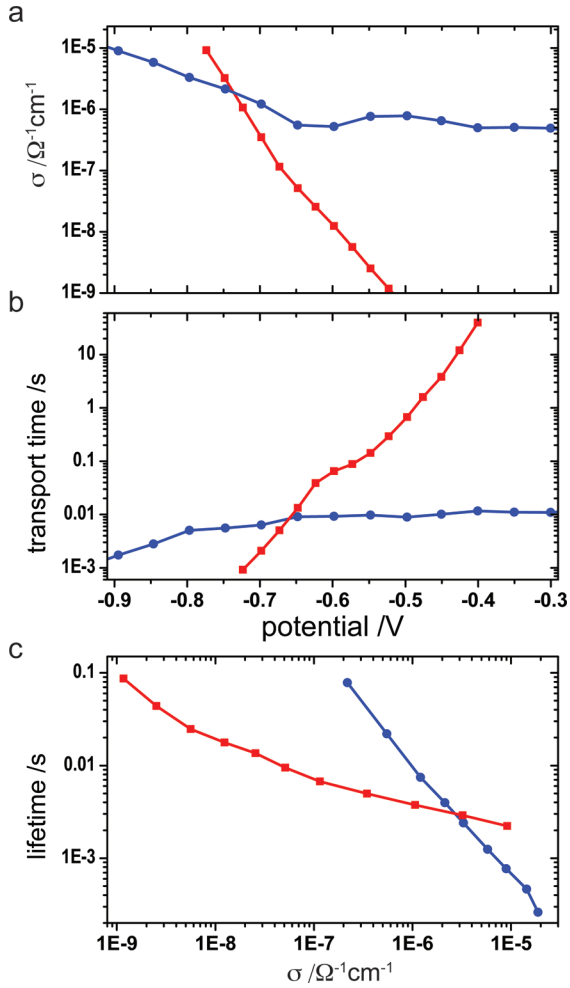


**Figure 4. Electrochemical impedance spectroscopy in the dark. (a) Comparison of the conductivity in ss-DSCs made with conventional nanoparticles (red) and with the 3D fibrous network (blue). (b) Comparison of the transport time and (c) of the electron lifetime in the same respective ss-DSCs.**

port material, *tert*-butyl pyridine, and lithium bis(trifluoromethylsulfonyl)imide salt in chlorobenzene. To do so, each film is covered by a small quantity (50−70 μL) of the spiro-MeOTAD solution before spin coating at 1200 rpm for 45 s in order to maximize pore filling.[14] After spin coating, a 100 nm gold counter electrode was applied by thermal evaporation (see Supporting Information, Figure S5). Figure 3 shows the $J-V$ for the bare 3D fibrous network ss-DSCs as well as for cells which have been treated in aqueous acidic $TiCl_4$ or by atomic layer deposition (ALD) of $TiO_2$ (<1 nm) to improve interconnectivity.

The photocurrent for the bare nanowire-based thin film is significantly increased from 3.1 to 8.0 and 8.5 mA/cm$^2$ for the $TiCl_4$ and ALD-treated films, respectively. This increase results from an improved connectivity between the nanorods' aggregates. Additionnaly, ALD-treated films present a slightly improved fill factor and photovoltage (FF = 0.63, $V_{oc}$ = 838 mV) when compared to the bare and $TiCl_4$-treated film (FF = 0.56, $V_{oc}$ = 795 mV). Further investigations are ongoing in order to better understand the slight advantage of ALD deposition *versus* the conventional $TiCl_4$ treatment for 3D fibrous network-based ss-DSCs. Figure 3b shows the characterisitic dark shunt resistance is visible in the $J-V$ curves of the different cells which is due to nanorods sticking through the thin spiro-MeOTAD overlayer and contacting the gold counter electrode (Supporting Information, Figure S5 inset). This contributes to a slightly lower than expected fill factor when compared to that of conventional nanoparticle ss-DSCs which is closer to FF ≈ 0.70.[8] Finally, the 3D single-crystalline network of anatase nanorods gives an overall power conversion efficiency of 4.9% which is close to the published efficiency record of 5% for a solid-state spiro-MeOTAD DSC.[8]

In this work, the electrical behavior of the 3D fibrous network spiro-MeOTAD-based ss-DSCs was studied by electrochemical impedance spectroscopy. The impedance spectra were analyzed using the transmission line model.[10,34−36] One advantage of this method is that it enables the direct comparison of electronic parameters like conductivity of the $TiO_2$, transport time, and lifetime of electrons in conventional nanoparticle-based films and in the 3D fibrous network ss-DSCs. In particular, the latter is compared to a nanoparticle-based cell sensitized with the same C218 dye and with very similar photovoltaic performances (FF = 0.69, $V_{oc}$ = 810 mV, $J_{sc}$ = 8.2 mA/cm$^2$, $n$ = 5.4%). In order to prevent the light-induced variation of the spiro-MeOTAD doping level during impedance measurements, all parameters presented were obtained in the dark.

First, it can be seen that the conductivity of the 3D fibrous network is higher than its nanoparticle counterpart up to about 750 mV (Figure 4a). The conductivity of the fibrous network stays constant over a wide range of applied potential. This indicates a high doping density which is most probably caused by hydrogen intercalation during the nanowire synthesis.[37] The higher doping level was determined by the Mott−Schottky plots, which confirmed up to an order of magnitude higher charge carrier concentration in the 3D fibrous network and a shift of the flat band potential to higher forward bias.[38] Likewise, the transport time in the 3D fibrous network can be up to several orders of magnitude shorter than that in the nanoparticle-based film, especially at lower bias potentials (Figure 4b). This result clearly confirms that the nanowires have an advantage in electron transport when compared to a conventional nanoparticle film. This is in part the result of the higher doping density in the films, but it is also most probably due to the longer diffusion length of the electron before having to hop on another nanowire.[39] Finally, the comparison of the electron lifetime shows the same tendency (Figure 4c). At low potentials (or low $TiO_2$ conductivity), the 3D fibrous network ss-DSC shows a longer lifetime than that measured in the nanoparticle-based cell. At 750−800 mV (or $\sim 3 \times 10^{-6}$ $\Omega^{-1}$ $cm^{-1}$), the electron lifetime in the 3D fibrous network drops below that measured in the nanoparticle-based ss-DSCs. These measurements confirm the high quality of the anatase fibrous network in terms of crystallinity and electronic properties. The superior light scattering as well as the shorter transport time and longer electron lifetime at the maxium power point contribute to a higher photocurrent and charge collection efficiency in the ss-DSC. These favorable optical and electronic characteristics help explain the high-power conversion efficiency obtained with this novel morphology in spite of the lower dye loading.

## CONCLUSION

In conclusion, the first high-efficiency ss-DSC built using a 3D fibrous network of anatase nanowires self-assembled from fused single-crystal nanorods was presented. This novel photoanode material is the first to incorporate a high-conductivity network for efficient electron extraction, a high roughness factor for dye loading, and large pores for enhanced light harvesting through light scattering. XRD, HRSEM, and TEM were used to show that the primary protonated titanate nanorods spontaneously orient themselves and self-assemble into secondary nanowires of joined particles with optimized anatase crystallographic orientations. This morphology offers large pores that efficiently scatter light to enhance light harvesting and a high roughness factor of 144 that permits good dye loading. Through a detailed study using electrochemical impedance spectroscopy, it was confirmed that this 3D morphology presents a significantly higher conductivity, shorter transport time, and longer electron lifetime over a wide range of applied potential than comparable nanoparticle-based ss-DSCs which result in improved collection efficiencies. Ultimately, these factors combine to give the highest recorded power conversion efficiency in a nanowire-based solid-state device of 4.9% (AM1.5). This novel 3D network of single-crystalline nanowires presents morphological and electronic characteristics that put it in direct competition with conventional nanoparticle-based ss-DSCs, which are now capable of achieving only slightly higher power conversions of 5% (AM1.5).

## METHODS

**Nanowire Synthesis.** In a typical synthesis, 3.7 g of titanium(IV) oxide nanopowder (99.7% anatase, Aldrich) is mixed with 35 mL of 10 M NaOH (97% Aldrich) solution. The mixture is then transferred into a Teflon-lined stainless steel autoclave (Parr Instrument Company) and heated at 130 °C for 36 h. After this treatment, the autoclave is left to cool to room temperature at a rate of 1 °C $min^{-1}$. The supernatant is gently decanted from the cake-like half-product that is formed at the bottom of the Teflon linear. Then, 35 mL of 15 M KOH (Fluka) solution is immediately added and the temperature is increased gradually (3 °C $min^{-1}$) to 200 °C for 24 h. The system is cooled to 150 °C at a rate of 1 °C $min^{-1}$ and subsequently kept at 150 °C for 12 h. The autoclave is then quenched to room temperature. The white product is then collected, filtered, and washed several times with deionized water and neutralized with the appropriate amount of 0.1 M HCl solution (Merck). It is then washed with hot (80 °C) deionized water in order to remove remaining traces of NaCl and KCl. The white powder is finally dried at 100 °C for 6 h in air. The obtained product is gently ground evacuated at 250 °C for 4 h in vacuum to complete the drying.

**Nanowire Suspension.** Nanowire powder (2.4 g) is dispersed in 100 mL of 2-propanol (>99.8% Merck), and the mixture is homogenized with an ultrasonic tip (Bandelin Sonopuls, Microtip MS73) 10% amplitude for 30 min.

**Titanate Nanowire Decomposition.** Once deposited on the FTO glass substrates by doctor blading, the samples are heat treated at 600 °C in air for 2 h. Titanate nanowires crytallize into anatase structure as confirmed by the X-ray diffractograms presented in Figure S1. The nanowires can be described as a chain-like assembly of $TiO_2$ nanorods with morphological characteristics presented in Figure S2.

**Solid-State Dye-Sensitized Solar Cell Fabrication.** Complete DSC devices were prepared using 2.5 μm doctor bladed thin films on FTO glass (TEK15, 15 Ω/□) covered with a 100 nm compact layer of $TiO_2$ deposited by spray pyrolysis to avoid recombination losses with the hole transport material. After calcination in air at 600 °C for 2 h, interconnectivity within the 3D network of nanowires was improved by treating the photoanodes in aqueous acidic $TiCl_4$ (40 mM, 70 °C, 30 min) or atomic layer deposition (ALD) of titanium tetraisopropoxide (<1 nm, 200 °C). The photoanodes are then dipped overnight in a $1 \times 10^{-4}$ M acetonitrile solution of C218 high extinction coefficient organic dye.[29] The thin film is then infiltrated with a solution of spiro-MeOTAD hole transport material (Merck Gmbh, 180 mg/mL), *tert*-butyl pyridine (1:26 mL $mg^{-1}$ tbp/spiro-MeOTAD), lithium bis(trifluoromethylsulfonyl)imide salt (Li-TFSI, 170 mg $mL^{-1}$ acetonitrile solution, 1:12 mL $mg^{-1}$ of Li-TFSI solution/spiro-MeOTAD) in chlorobenzene. To do so, each nanowire-based thin film is first covered with 50−70 μL of the spiro-MeOTAD solution before

spin coating and left for 40 s before spin coating at 1200 rpm for 45 s in order to maximize pore filling.[14] After spin coating, the counter electrode was applied by thermal evaporation of 100 nm of gold. $J-V$ measurements of the cell were carried out under standardized AM1.5 illumination of 100 mW/cm$^2$ (active area 0.18−0.19 cm$^2$, spectral mismatch 2%).

**Electrochemical Impedance Spectroscopy Measurements.** The electrochemical impedance spectroscopy (EIS) measurements of the samples were performed at 20 °C using a sinusoidal potential perturbation of 10 mV, which was applied over a frequency range from 1 MHz down to 0.1 Hz (Autolab PG30). Measurements were analyzed using the transmission line model from Bisquert *et al.*[10,35]

*Acknowledgment.* This publication was supported by the King Abdullah University of Science and Technology (KAUST, Award No KUS-C1-015-21). J.B. received financial support from a Marie Curie Research Training Network, Hydrogen Project (MRTN-CT-2006-032474). N.C. and P.W. thank the financial support from the National Key Scientific Program (No. 2007CB936700) and the National Science Foundation of China (No. 50973105). This work was partially supported by the european project MULTIPLAT (NMP4-SL-2009-228943). T.M. acknowledges the ECR advanced grant agreement (No. 247404) under the CE-Mesolight project funded by the European community's 7th FWP.

*Supporting Information Available:* Additional figures and table. This material is available free of charge *via* the Internet at http://pubs.acs.org.

## REFERENCES AND NOTES

1. Chiba, Y.; Islam, A.; Watanabe, Y.; Komiya, R.; Koide, N. Dye-Sensitized Solar Cells with Conversion Efficiency of 11.1%. *Jpn. J. Appl. Phys.* **2006**, *45*, L638–L640.
2. Gao, F.; Wang, Y.; Shi, D.; Zhang, J.; Wang, M.; Jing, X. Enhance the Optical Absorptivity of Nanocrystalline $TiO_2$ Film with High Molar Extinction Coefficient. *J. Am. Chem. Soc.* **2008**, *130*, 10720–10728.
3. Graetzel, M. The Advent of Mesoscopic Injection Solar Cells. *Prog. Photovoltaics* **2006**, *14*, 429–442.
4. Snaith, H.; Schmidt-Mende, L. Advances in Liquid-Electrolyte and Solid-State Dye-Sensitized Solar Cells. *Adv. Mater.* **2007**, *19*, 3187–3200.
5. Yanagida, S.; Yu, Y.; Manseki, K. Iodine/Iodide-Free Dye-Sensitized Solar Cells. *Acc. Chem. Res.* **2009**, *42*, 1827–1838.
6. Bach, U.; Lupo, D.; Comte, P.; Moser, J.; Weissörtel, F; Salbeck, J.; Spreitzer, H.; Gratzel, M. Solid-State Dye-Sensitized Mesoporous $TiO_2$ Solar Cells with High Photon-to-Electron Conversion Efficiencies. *Nature* **1998**, *395*, 583–585.
7. Snaith, H. J.; Moule, A. J.; Klein, C.; Meerholz, K.; Friend, R. H.; Gratzel, M. Efficiency Enhancements in Solid-State Hybrid Solar Cells *via* Reduced Charge Recombination and Increased Light Capture. *Nano Lett.* **2007**, *7*, 3372–3376.
8. Wang, M.; Liu, J.; Cevey-Ha, N.; Moon, S.; Liska, P.; Humphry-Baker, R.; Moser, J.; Gratzel, C.; Wang, P.; Zakeeruddin, S.; *et al.* High Efficiency Solid-State Sensitized Heterojunction Photovoltaic Device. *Nano Today* **2010**, *5*, 169–174.
9. Schmidt-Mende, L.; Zakeeruddin, S.; Gratzel, M. Efficiency Improvement in Solid-State-Dye-Sensitized Photovoltaics with an Amphiphilic Ruthenium-Dye. *Appl. Phys. Lett.* **2005**, *86*, 013504.
10. Fabregat-Santiago, F.; Bisquert, J.; Cevey, L.; Chen, P.; Wang, M.; Zakeeruddin, S. M.; Graetzel, M. Electron Transport and Recombination in Solid-State Dye Solar Cell with Spiro-Ometad as Hole Conductor. *J. Am. Chem. Soc.* **2009**, *131*, 558–562.
11. Jennings, J. R.; Peter, L. M. A Reappraisal of the Electron Diffusion Length in Solid-State Dye-Sensitized Solar Cells. *J. Phys. Chem. C* **2007**, *111*, 16100–16104.
12. Kruger, J.; Plass, R.; Gratzel, M.; Cameron, P.; Peter, L. Charge Transport and Back Reaction in Solid-State Dye-Sensitized Solar Cells: A Study Using Intensity-Modulated Photovoltage and Photocurrent Spectroscopy. *J. Phys. Chem. B* **2003**, *107*, 7536–7539.
13. Snaith, H.; Grätzel, M. Electron and Hole Transport through Mesoporous $TiO_2$ Infiltrated with Spiro-MeOTAD. *Adv. Mater.* **2007**, *19*, 3643–3647.
14. I.-K., D.; Tétreault, N.; Brillet, J.; Hardin, B. E.; Smith, E. H.; Rosenthal, S. J.; Sauvage, F.; Grätzel, M; McGehee, M. D. Pore-Filling of Spiro-Ometad in Solid-State Dye Sensitized Solar Cells: Quantification, Mechanism, and Consequences for Device Performance. *Adv. Funct. Mater.* **2009**, *19*, 2431–2436.
15. Dloczik, L.; Ileperuma, O.; Lauermann, I.; Peter, L.; Ponomarev, E.; Redmond, G.; Shaw, N.; Uhlendorf, I. Dynamic Response of Dye-Sensitized Nanocrystalline Solar Cells: Characterization by Intensity-Modulated Photocurrent Spectroscopy. *J. Phys. Chem. B* **1997**, *101*, 10281–10289.
16. Kopidakis, N.; Schiff, E.; Park, N.; van de Lagemaat, J.; Frank, A. Ambipolar Diffusion of Photocarriers in Electrolyte-Filled, Nanoporous $TiO_2$. *J. Phys. Chem. B* **2000**, *104*, 3930–3936.
17. van de Lagemaat, J.; Zhu, K.; Benkstein, K. D.; Frank, A. J. Temporal Evolution of the Electron Diffusion Coefficient in Electrolyte-Filled Mesoporous Nanocrystalline $TiO_2$ Films. *Inorg. Chim. Acta* **2008**, *361*, 620–626.
18. Wang, Q.; Ito, S.; Graetzel, M.; Fabregat-Santiago, F.; Mora-Sero, I.; Bisquert, J.; Bessho, T.; Imai, H. Characteristics of High Efficiency Dye-Sensitized Solar Cells. *J. Phys. Chem. B* **2006**, *110*, 25210–25221.
19. Martinson, A. B. F.; Elam, J. W.; Liu, J.; Pellin, M. J.; Marks, T. J.; Hupp, J. T. Radial Electron Collection in Dye-Sensitized Solar Cells. *Nano Lett.* **2008**, *8*, 2862–2866.
20. Law, M.; Greene, L.; Johnson, J.; Saykally, R.; Yang, P. Nanowire Dye-Sensitized Solar Cells. *Nat. Mater.* **2005**, *4*, 455–459.
21. Martinson, A. B. F.; Elam, J. W.; Hupp, J. T.; Pellin, M. J. Zno Nanotube Based Dye-Sensitized Solar Cells ZnO Nanotube Based Dye-Sensitized Solar Cells. *Nano Lett.* **2007**, *7*, 2183–2187.
22. Mor, G.; Shankar, K.; Paulose, M.; Varghese, O.; Grimes, C. Use of Highly-Ordered $TiO_2$ Nanotube Arrays in Dye-Sensitized Solar Cells. *Nano Lett.* **2006**, *6*, 215–218.
23. Chen, P.; Brillet, J.; Bala, H.; Wang, P.; Zakeeruddin, S. M.; Graetzel, M. Solid-State Dye-Sensitized Solar Cells Using $TiO_2$ Nanotube Arrays on FTO Glass. *J. Mater. Chem.* **2009**, *19*, 5325–5328.
24. Kay, A.; Gratzel, M. Low Cost Photovoltaic Modules Based on Dye Sensitized Nanocrystalline Titanium Dioxide and Carbon Powder. *Sol. Energy Mater. Sol. Cells* **1996**, *44*, 99–117.
25. Chen, D.; Huang, F.; Cheng, Y.-B.; Caruso, R. A. Mesoporous Anatase $TiO_2$ Beads with High Surface Areas and Controllable Pore Sizes: A Superior Candidate for High-Performance Dye-Sensitized Solar Cells. *Adv. Mater.* **2009**, *21*, 2206–2210.
26. Halaoui, L.; Abrams, N.; Mallouk, T. Increasing the Conversion Efficiency of Dye-Sensitized $TiO_2$ Photoelectrochemical Cells by Coupling to Photonic Crystals. *J. Phys. Chem. B* **2005**, *109*, 6334–6342.
27. Mihi, A.; Calvo, M. E.; Anta, J. A.; Miguez, H. Spectral Response of Opal-Based Dye-Sensitized Solar Cells. *J. Phys. Chem. C* **2008**, *112*, 13–17.
28. Guldin, S.; Huttner, S.; Kolle, M.; Welland, M. E.; Mueller-Buschbaum, P.; Friend, R. H.; Steiner, U.; Tetreault, N. Dye-Sensitized Solar Cell Based on a Three-Dimensional Photonic Crystal. *Nano Lett.* **2010**, *10*, 2303–2309.
29. Li, R.; Liu, J.; Cai, N.; Zhang, M.; Wang, P. Synchronously Reduced Surface States, Charge Recombination, and Light Absorption Length for High-Performance Organic Dye-Sensitized Solar Cells. *J. Phys. Chem. B* **2010**, *114*, 4461–4464.
30. Penn, R.; Banfield, J. Morphology Development and Crystal Growth in Nanocrystalline Aggregates under Hydrothermal Conditions: Insights from Titania. *Geochim. Cosmochim. Acta* **1999**, *63*, 1549–1557.

31. Zhang, Q.; Liu, S.-J.; Yu, S.-H. Recent Advances in Oriented Attachment Growth and Synthesis of Functional Materials: Concept, Evidence, Mechanism, and Future. *J. Mater. Chem.* **2009**, *19*, 191–207.
32. Alimohammadi, M.; Fichthorn, K. A. Molecular Dynamics Simulation of the Aggregation of Titanium Dioxide Nanocrystals: Preferential Alignment. *Nano Lett.* **2009**, *9*, 4198–4203.
33. Wang, P.; Zakeeruddin, S.; Comte, P.; Charvet, R.; Humphry-Baker, R.; Gratzel, M. Enhance the Performance of Dye-Sensitized Solar Cells by Co-Grafting Amphiphilic Sensitizer and Hexadecylmalonic Acid on $TiO_2$ Nanocrystals. *J. Phys. Chem. B* **2003**, *107*, 14336–14341.
34. Bisquert, J. Theory of the Impedance of Electron Diffusion and Recombination in a Thin Layer. *J. Phys. Chem. B* **2002**, *106*, 325–333.
35. Bisquert, J.; Garcia-Belmonte, G.; Fabregat-Santiago, F.; Compte, A. Anomalous Transport Effects in the Impedance of Porous Film Electrodes. *Electrochem. Commun.* **1999**, *1*, 429–435.
36. Fabregat-Santiagoa, F.; Bisquert, J.; Palomares, E.; Haque, S. A.; Durrant, J. R. Impedance Spectroscopy Study of Dye-Sensitized Solar Cells with Undoped Spiro-Ometad as Hole Conductor. *J. Appl. Phys.* **2006**, *100*, 034510.
37. Di Valentin, C.; Pacchioni, G.; Selloni, A. Reduced and N-Type Doped $TiO_2$: Nature of $Ti^{3+}$ Species. *J. Phys. Chem. C* **2009**, *113*, 20543–20552.
38. Bisquert, J.; Garcia-Belmonte, G.; Fabregat-Santiago, F. Modelling the Electric Potential Distribution in the Dark in Nanoporous Semiconductor Electrodes. *J. Solid State Electron.* **1999**, *3*, 337–347.
39. Nakade, S.; Matsuda, M.; Kambe, S.; Saito, Y.; Kitamura, T.; Sakata, T.; Wada, Y.; Mori, H.; Yanagida, S. Dependence of $TiO_2$ Nanoparticle Preparation Methods and Annealing Temperature on the Efficiency of Dye-Sensitized Solar Cells. *J. Phys. Chem. B* **2002**, *106*, 10004–10010.